Journal Name

ARTICLE

High-Quality Perovskite Films via Post Annealing Microwave Treatment

Received 00th January 20xx,
Accepted 00th January 20xx

DOI: 10.1039/x0xx00000x

www.rsc.org/

Kai-Li Wang [a], Cong-Cong Zhang [a], Yu-Rong Jiang [a], Hai-Rui Liu [a], Xiao-Mei Li [a], Sagar M. Jain* [b] and Heng Ma*[a]

Abstract: Crystalline quality of the perovskite film plays a key role in improving the optoelectronic properties and performance of planar perovskite hybrid solar cells (PSCs). In this work, a methodology employing post-annealing microwave treatment (MPAT) for fine tuning the crystallization of perovskite films is proposed. It is found that microwave induced electromagnetic waves results in the dipoles and ions to vibrate at high frequency in perovskite crystals, which catalyzes Ostwald ripening process resulting in a good quality perovskite films. High quality perovskite films are obtained when subjected to MPAT of 350 watts power for 25 seconds. The resulting films in inverted solar cell architecture shown champion efficiency of 13.39%. This is significant improved performance over devices employing films without MPAT treatment (PCE=11.5%). The MPAT paves a way to prepare high quality perovskite films that is of particularly significance for manufacturing of the large area perovskite solar cells.

1. Introduction

In only few years of timespan, perovskite solar cells (PSCs) have reached dazzling achievements. The photovoltaic power conversion efficiency (PCE) increased from 3.8% to 23.3% [1] and is very close to the theoretical efficiency of ~31%.[2, 3]

The photovoltaic performance of PSCs is not only attributed to the morphology[5, 6] and composition[7] of the perovskite films but also to the charge extracting capacity of the hole and electron transporting layers.[8-10] Homogeneous thermal gradient over entire area of substrate is one of the key factor deciding the quality of the perovskite film.[11, 12]

Wang et al used imidazole doping treatment for PEDOT:PSS hole transport layer to tune the PH value that leads to enhanced power conversion efficiency of 15% for $CH_3NH_3PbI_3$ based inverted perovskite solar cells[4] However, for $CH_3NH_3PbI_{3-x}Cl_x$ perovskite absorber with an inverted architecture the efficiency still lacks behind. For $CH_3NH_3PbI_{3-x}Cl_x$, it is reported that the film is annealed at 100°C for 90 min.[13] However, the conventional hot plate annealing process often suffers from inhomogeneous thermal gradients for large area giving inhomogeneous crystallization for perovskite films resulting into poor reproducibility for high efficiency solar cells.[20,34] Recently, in this direction alternative processes are developed to replace traditional annealing process. These includes - hot-pressing,[14] solvent annealing [15, 16] IR radiation[17] and ultrasonic vibration[18-20]. Unfortunately, all these methods are time-consuming. Therefore, it is of key importance and timely to find alternative methods on the conventional annealing technology. Here we

[a] *Department of Henan Province Key Laboratory of Photovoltaic Materials& College of Physics & Materials Science, Henan Normal University, Xinxiang 453007, China.* *E-mail address: hengma@henannu.edu.cn*

[b] *SPECIFIC, College of Engineering, Swansea University Bay Campus, Fabian Way, SA1 8EN Swansea, United Kingdom.* *E-mail address: sagarmjain@gmail.com , s.m.jain@swansea.ac.uk*

proposed, a microwave post-annealing treatment (MPAT) that can generate more homogeneous thermal domain to evaporate the solvent and the co-associated high frequency vibration can improve the Oswald ripening process by fusing the smaller crystals into the large crystallites.[35,36] Microwave is form of electromagnetic radiation with wavelengths ranging from one-meter to one millimeter.[21-23] In last 30 years, microwave treatment technology have a breakthrough achievement in photoelectron manufacturing.[24-27] For example, the microwave technology has improved heating rate and thermal efficiency and most strikingly solved the problem of uneven heating over a large area.[28-30] On the other hand, the electromagnetic can supply a vibration of electrons and dipoles for the atoms present in the absorber layer.[31] For perovskite absorber annealing process, microwave technology is ideal to provide a more homogeneous and high-efficiency thermal annealing environment[32,33]

It is reported that the microwave irradiation can bring many functions.[31,36-38] Earlier, Cao et al reported the use of microwave irradiation for obtaining good quality $CH_3NH_3PbI_3$ perovskite films that resulted into 14.91% device efficiency.[39] Considering the difficulty involved in tuning chlorine/iodine ratio[40,41]. In this work we demonstrated the use of microwave post-annealing treatment (MPAT) to form good quality mixed halide $CH_3NH_3PbI_{3-x}Cl_x$ perovskite films. Applied MPAT resulted in more homogeneous thermal domain to evaporate the solvent and at the same time the co-associated high frequency vibration can improve the Oswald ripening process by fusing the smaller crystals into the large crystallites[35,36] Unlike the conventional annealing process at 100°C for 90 minutes, MPAT involves microwave post-annealing treatment (MPAT) where a perovskite absorber radiated with microwave based on the thermal annealing at 100°C for 70 minute. In this hybrid processing treatment, microwave treatment allows the formation of the homogeneous perovskite catalytic grains at regular intervals and the annealing enhance the high quality crystal growth.

$CH_3NH_3PbI_{3-x}Cl_x$ perovskite films prepared using MPAT shown homogeneous and high quality crystalline growth as confirmed from X-ray diffraction, UV-visible and surface morphology characterization and as a result on employing in solar cells yields champion performance of 13.39 % this is much higher performance than the devices made using conventional annealing (efficiency of 11.58%).

2. Materials and methods

2.1. Materials and Preparation

Poly (3, 4-ethylene-dioxythiophene): polystyrene sulfonate (PEDOT: PSS) were purchased from Heraeus (Germany); Lead (II) chloride ($PbCl_2$) (99.999%), and anhydrous N, N-dimethylformamide (DMF) (99.9%) were purchased from Alfa-Aesar; PCBM and Bphen were produced by Nichem Fine Technology Co., Ltd. (Taiwan).

Methylamine Iodide synthesis (CH_3NH_3I) : 20 ml of hydroiodic acid (57 wt% in H_2O) was added to 48mL methanol (40 wt%) under ice bath stirring for 2 h. and then, the reactants solution was distilled in the rota- evaporator at 55 °C to remove the solvents, the precipitate was washed by diethyl ether 3 times. Finally, white powder was collected and dried at 60 °C for 24 h in vacuum.

Perovskite precursor solution preparation : The mixture of $PbCl_2$:CH_3NH_3I with 1:3 molar ratios was dissolved in DMF and then stirred at 60 °C overnight. The solution was filtered using 0.45 µm filter and directly used for spin coating.

Microwave equipment : For microwave irradiation Whirlpool MAX39 equipment is used (**Figure S1).** The selected power of the microwave radiation can be tuned to 150W, 350W and 500 W.

2.2. Solar cell fabrication

ITO-coated glass substrate (15 Ω/sq) was ultrasonic-coated in acetone and ethanol at room temperature for 20 min. Followed by the UV-Ozone clean for 15 minute. PEDOT:PSS films of thickness ≈ 45 was spin-coated onto ITO substrate at 4500 rpm and annealed at 140 °C for 25 min. The as prepared perovskite precursor solution was spin-coated at 4000 rpm. For the reference cell the conventional

thermal annealing process were employed to prepare perovskite films. This involves gradual temperature increment from 60 to 100 °C at a rate of 10°C/10 minutes and then the cell is subjected to annealing on the hot plate for 90 minutes. For MPAT processed perovskite films. The cell was also annealed at 100°C like the reference device but the followed placement time is 70 minutes instead of 90 minute on the hot plate. The cells placed 70 minute were irradiated with microwave in a confined glass chamber purged with nitrogen environment. As the microwave power and the irradiated time can strongly influence the quality of perovskite film. Number of sets were tried to irradiate the perovskite films using microwave. It is found that the sets of 160w-30s, 350w-25s and 500w-15s results into good reproducibility for obtaining high quality perovskite films. Once the perovskite films are deposited. PCBM layer is deposited using 20 mg/ml in chlorobenzene solution at 2000 rpm. 0.5 mg/ml Bphen in absolute ethanol was coated onto PCBM layer at 4000 rpm. Finally, 100 nm thick Ag (mask area of 0.0725 cm^2) was deposited on top of the Bphen layer by thermal evaporation under 10^{-4} Torr.

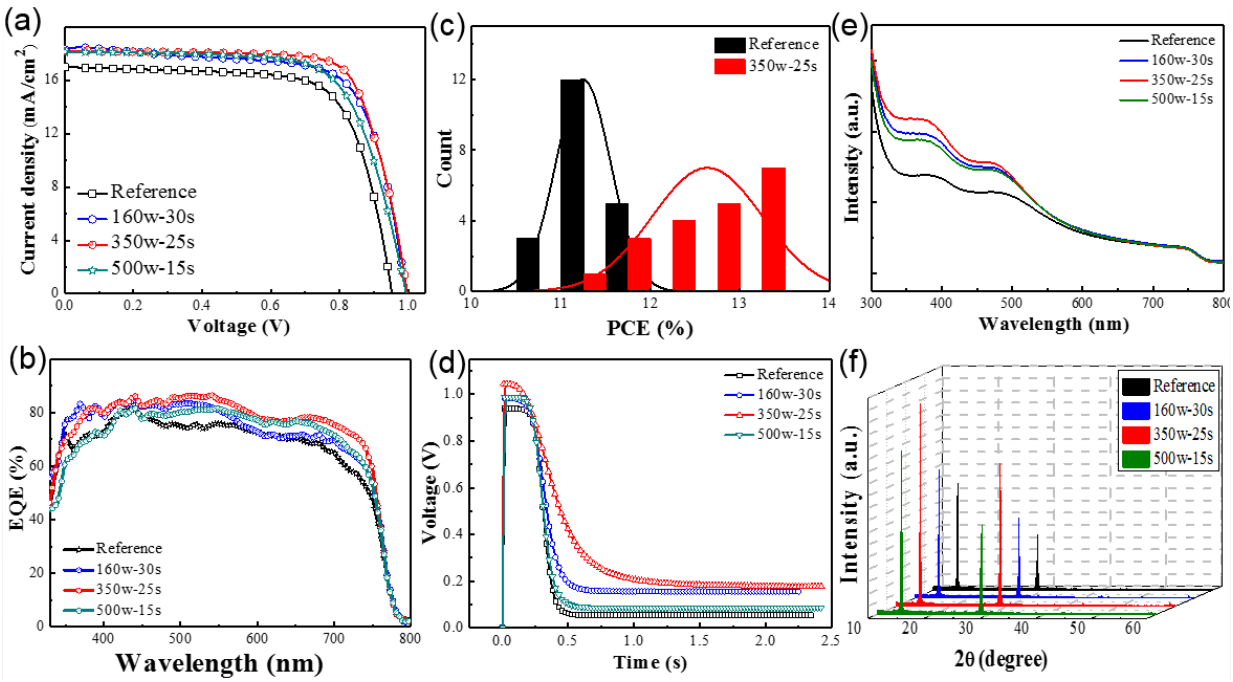

Fig.1. The photovoltaic performance and optoelectronic properties of perovskite solar devices employing perovskite absorber prepared with and without MPAT processing. (a) *J-V* characteristics of perovskite solar cells under standard 1 sun (AM 1.5G, 100 mW/cm^2) illumination condition. (b) IPCE / EQE of respective perovskite devices. (c) Efficiency distribution histograms of the perovskite solar cells. (d) Open circuit voltage decay (OCVD) for the respective perovskite devices. (e) UV-Vis absorption spectra and (f) X-ray diffraction patterns for perovskite films with and without MPAT treatment.

Table 1. Photovoltaic performance parameters at 1000 Wm^{-2} (AM 1.5G) of PSCs prepared with and without microwave treatment (reference) and PSCs with 160 w-30s, 350 w-25s and 500 w-15s microwave treatment.

Device	*Voc* (V)	*Jsc* (mA/cm²)	FF (%)	PCE (%)	PCE_{best} (%)
Reference	0.96±0.01	16.56±0.37	0.71 ±0.01	11.16±0.27	11.58
160w-30s	0.96±0.01	17.25±0.29	0.73±0.01	11.95±0.26	12.94
350w-25s	0.99±0.01	17.70±0.52	0.74 ±0.01	12.83 ±0.42	13.39
500w-15s	0.98±0.01	17.12±0.52	0.72±0.01	11.93 ±0.41	12.54

2.3. Characterization

Perovskite solar cells fabricated on ITO/PEDOT:PSS/Perovskite/BCP/PCBM/Au architecture. The *J-V* characteristics, Open-circuit voltage decay (OCVD) response and Dark current were tested by a programmable Keithley 2400 source meter under AM 1.5 G illumination with light intensity of 100 mW/cm² (Newport, Class AAA solar simulator, 94023A-U). Incident-photon-to-current efficiency (IPCE) was measured by 1000 W halogen lamp and grating monochromator (Acton Spectra Pro 2300i). The electrochemical impedance spectroscopy (EIS) was surveyed by an IM6e Electrochemical work station (ZAHNER, Germany). The dielectric constant ε_r and corresponding dissipation factor δ as a function of frequency were measured by precision impedance analyser (Agilent 4294A). The absorption spectra were measured with an UV-Vis spectrophotometer (PerkinElmer Lambda 750). The surface and cross-sectional morphology were characterized by scanning electron microscopy (SEM, Quanta 200 FEG, FEI Co.). X-ray diffraction (XRD) pattern was measured using PAN Analytica 80 equipment (Empyrean, Cu Kα radiation with a wavelength of 0.154 nm). In order to evaluate the solar cell stability. The non-encapsulated devices were exposed to ambient air.

3. Results and discussion

The films subjected to MPAT (160w-30s, 350w-25s and 500w-15s) shows enhanced crystallization and absorbance as compare to the films prepared using conventional annealing (reference devices) this is evidenced from enhanced X-ray diffraction and ultraviolet visible absorbance (Figure 1 (e-f)). It is found that devices prepared using MPAT processed films shows improved *JV* characteristics as compare to the reference devices. The *JV* characteristics and EQE measurements are shown in Figure 1 (a-b).

Particularly, for the films subjected to 350w-25s MPAT processing shown highest performance of 13.39% hysteresis-free efficiency (*Jsc* = 17.70, *Voc* = 0.99 and fill factor = 0.74). While the reference perovskite cells shown PCE of 11.5% (*Jsc* = 16.56, *Voc* = 0.96 and fill factor = 0.71) with significant hysteresis. Statistic of 30 devices prepared with and without MPAT treatment perovskite films presented in Figure S5.

The IPCE curves of the PSCs with different annealing process are shown in **Figure 1b**. The devices prepared employing MPAT treatment obtain higher IPCE value in 300-800 nm wavelength range compare to the reference devices as a result of improved quality of the films after MPAT treatment. For MPAT 350w-25s, the integrating current density reached to 17.67 mA/cm² (Figure 1(a)), which is further confirmed from the *Jsc* value obtained from EQE measurements (Figure 1 (b)). The PCEs of the cells with MPAT at 350w-25s and reference cells presented in **Figure 1c**. Statistics 30

devices employing perovskite films processed with MPAT (350w-25s) shows narrow distribution indicating the excellent reproducibility of devices (Figure S5).

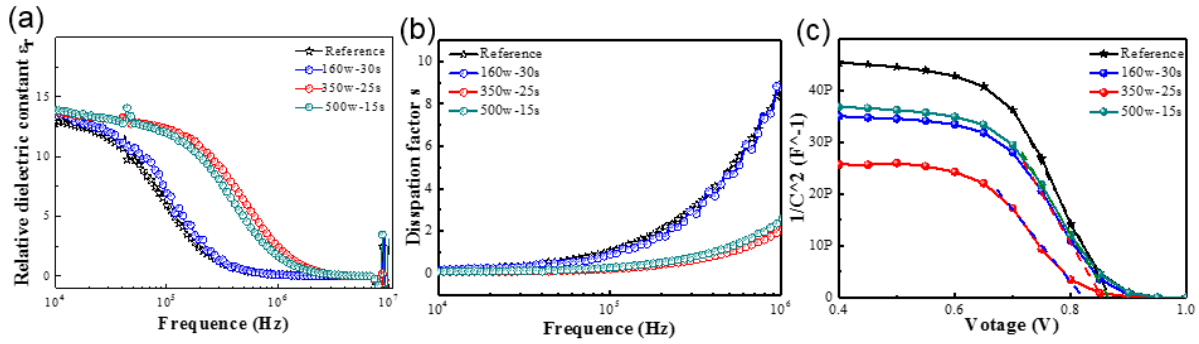

Fig.2. (a) Relative dielectric constant ε_r and (b) Corresponding dissipation factor δ as a function of frequency for the devices with MPAT under darkness at room temperature. (c) $1/C^2$ versus applied voltage graph of PSCs with and without MPAT.

Open-circuit voltage decay (OCVD) response time of the solar cell was used to investigate the photovoltage and charge recombination dynamics at the perovskite and PEDOT:PSS interface. As shown in **Figure 1d** the OCVD data of the cells includes three parts. (i) Forming of the photovoltage with illumination. As illustrated, the voltage with MPAT is larger than that of the reference devices. (ii) The decay time of the photovoltage with light shutter, which is defined as $\tau_{ir}(V) = (-\frac{1}{V}\frac{dV}{dt})^{-1}$ The voltage decay with MPATs takes longer time to reach a flat and steady value. It means that the more compact and smooth perovskite films are formed by MPAT can possibly be reducing the charge recombinations.[42,43,44] From the curves, the obtained lifetime of the photovoltage of the perovskite devices employing MPAT processed films is longer (0.45~1.2 s) than that of the reference cells (0.3 s). (iii) The dark recovery step gives information about enhanced electrostatic potential (V_{elec}) of the interface using the equation $V_{oc} = V_{bi} + V_{elec}$ [45]. Because of MPAT, the devices obtain a high $V_{elec,}$ which results in a high V_{oc}. The crystallization of the perovskite films is one of the key factor in the photoelectric performance of PSCs. Thus, we further characterized the perovskite films characteristics using ultraviolet-visible (UV-Vis) and wide-angle X-ray diffraction (XRD). The results are listed in **Figure 1e** and **1f**. For the UV-Vis absorption, the perovskite films with MPAT (350w-25s) shows the strongest absorption intensity,as well crystalline quality. Corresponding to XRD analysis, the main diffraction intensities of the MPAT film at 14.2° increase considerably, confirming the improved crystallinity of the perovskite films[46] .

Microwave is electromagnetic waves. Thus, the main effect of the electric component should be considered in this study. Dielectric relaxation is the momentary lag in the dielectric constant, which relate to the ionic or electronic polarization of the perovskite films. Therefore, the capacitance of the solar cells is measured as a function of frequency. **Figure 2a** and **2b** presents the dissipation factor (tan δ) and the relative dielectric constant (ε_r) of the PSCs with and without MPAT under darkness at room temperature. As mentioned earlier, MPAT can bring thermal annealing effect and the polarization

effect along the electric field of the microwave. This effect will result formation of highly ordered, homogeneous crystalline domains for MPAT processed films. From X-ray diffraction measurement of MPAT processed films shows enhanced crystal planes (110, 2ϑ=14.9°). The crystalline, homogeneous films can also bring an enhanced effect on the dielectric constant. From **Figures 2a** at low and high frequency,[47] the dielectric constant ε_r does not shows similar trend for the films prepared with and without MPAT processing. However, in the middle frequency the proper MPAT processed films bring obvious effect on the dielectric measurement. This is possibly due to the lower dissipation factors (tan δ) (**Figure 2b)**.

Table 2. The built-in potential and carrier density of perovskite devices prepared with or without MPAT by fitting linear part in *C-V*.

Device	Vbi (V)	ND (cm^{-3})
Reference	0.89	0.97 E16
160w-30s	0.87	1.18 E16
350w-25s	0.83	1.53 E16
500w-15s	0.87	1.40 E16

The measured capacitance as a function of forward bias (*C-V*) of the devices are summarized in **Figure 2c**, where the positive pole is set on ITO plate and the DC voltage swept from 0 V to 1.1 V at a frequency of 10 kHz. The capacitance can be written as[48]

$$\frac{1}{C^2} = \frac{2}{q\varepsilon A^2 N_D}\left(V_{bi} - V\right) \quad (1)$$

where q is the applied elementary charge, V is the applied forward bias, N_D is the carrier density and V_{bi} is the built-in potential. The inverse capacitance squared $1/C^2$ should be a linear function of V, whose intersection with the voltage axis yields the extrapolated V_{bi}.[49] and the slope of the linear region yields the N_D.[48] The detailed results are listed in Table 1. In the linear region, one can find that perovskite films with MPAT generate a decreased V_{bi}, but an increased N_D. For the reduced V_{bi}, the pre-polarization charge come from the bipolar perovskite molecules that forms the built in potential and is disturbed by the microwave in the MPAT process. The increase N_D also indicates that the defects in the perovskite film are less because of the high quality films obtained with MPAT processing. Furthermore, the increase N_D can give more large contribution to the $V_{elec.}$ Therefore with MPAT, the V_{oc} still shows increasing results compared to the reference cells although V_{bi} decreases (according to the equation $V_{oc} = V_{bi} + V_{elec}$)

Journal Name

ARTICLE

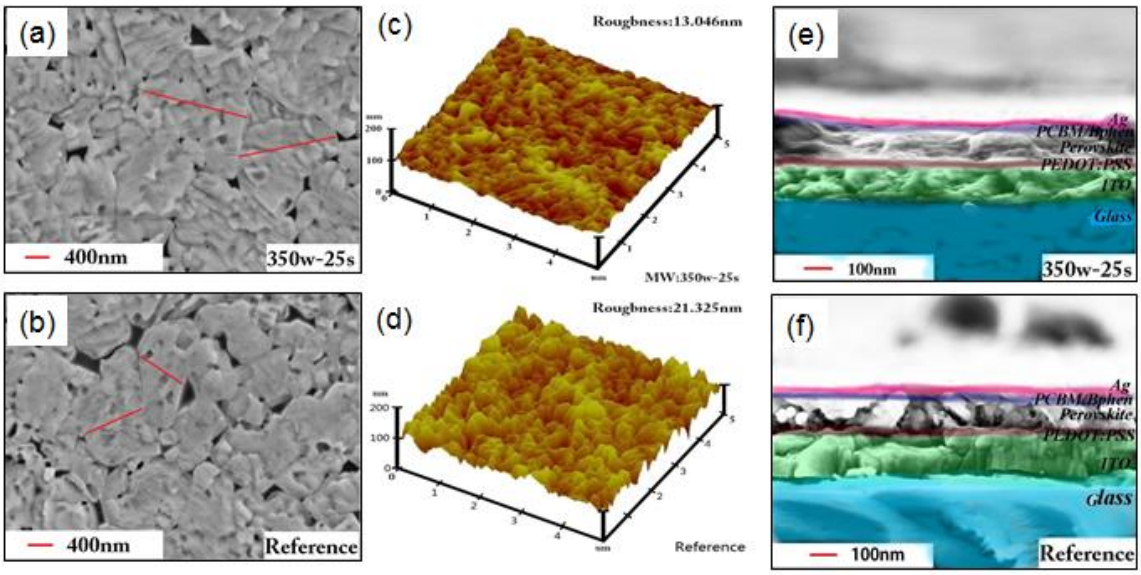

Fig.3. (a), (b) Top-view SEM images of perovskite films with (350w-25s) and without (reference) MPAT. (c), (d) 3-D AFM top-view micrographs of the perovskite films. (e), (f) SEM cross-section of respective photovoltaic devices prepared employing perovskite processed with MPAT and without MPAT.

Surface morphology SEM images and atomic force microscopy (AFM) images shows excellent quality for MPAT processed perovskite films. The top-view SEM images of perovskite films with and without MPAT processed are shown in **Figure 3a** and **3b**. For 350w-25s MPAT, a smooth - compact and pinhole free perovskite films are formed. Moreover, the mean grain size of the perovskite crystal was estimated using a Nano measure program. The statistic result is collected in **Figure S6**. It is found that the grain size of the film with MPAT (350w-25s) reaches 1538.96 nm, which is larger than the grain size of the reference films (943.35 nm). The three-dimensional (3-D) AFM micro-graphs of the films with and without MPAT processing presented in **Figure 3c** and **3d**. As illustrated, the root-mean-square (RMS) roughness of the perovskite film for MPAT (350w-25s) processed films is about 13 nm. Which is lower than that of the reference films (without MPAT processing) 21.3 nm. In summary, the SEM and AFM measurements further confirms that MPAT gives a high-quality perovskite films.

Journal Name

ARTICLE

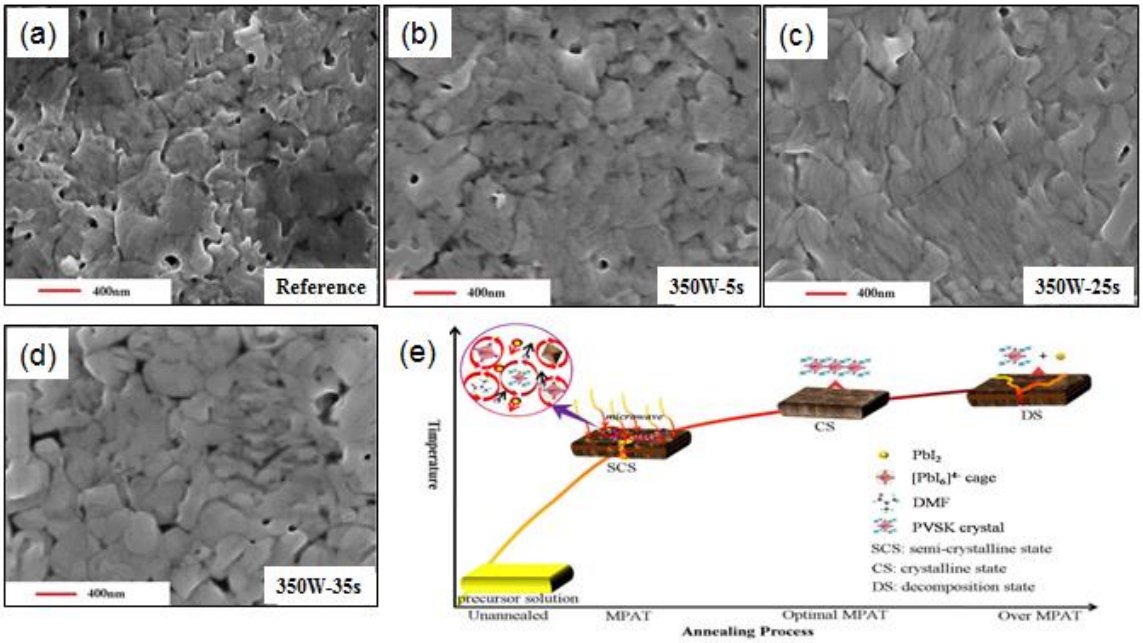

Fig. 4. Top-view SEM micrographs of perovskite films (a) Reference (without MPAT), and with MPAT (350 w) processing for different time (b) 5 s, (c) 25 s and (d) 35 s. (e) Schematic diagram of morphology evolution over time for perovskite film formed with MPAT processing.

Figure 3 (e-f) presents cross-sections of devices prepared without and with MPAT treatment respectively. Solar cell employing MPAT processed perovskite films shows more dense and thick monolithic perovskite absorber layer with less pinholes than perovskite films without MPAT treatment. The stability of the non-encapsulated solar cells prepared with and without MPAT processing was measured at 1 sun illumination and in ambient atmosphere (>25% humidity). The MPAT (350w-25s) processed perovskite devices exhibited better stability even after 240 hours of continuous 1 sun illumination. In contrast, the efficiency of reference devices prepared without MPAT treatment rapidly dropped by half just after 100 hours of illumination. (Figure S7) For the as deposited perovskite films there are un-evaporated DMF solvent, MA^+ cations and $[PbI_6]^{4-}$ cage nanoparticles. Therefore, MPAT and associated electromagnetic vibration can energetically prompt the small particles to fuse together leading to the large crystal grains. On the other hand, the electromagnetic vibration can also drive the hollow perovskite grain to become solid, which form more large and high-quality crystallization. As a result, the grain boundaries are seamed and pinholes are padded showing Oswald ripening.

Figure 4 and **Figure S8** Show the different SEM of the reference film and the MPAT film with 350 W at different time of reference film 5 s 25 s and 35s, respectively and the Corresponding UV-vis and XRD patterns are shown in Figure S9.[11,30,] One can find that the MPAT with

350 W 25s is the proper condition to form the Ostwald ripening crystal. However, increased MPAT time make perovskite to decompose into PbI_2 and MAI[12, 39] (Figure S10), leading to the appearance of pinholes. A schematic is presented in Figure 4e to show the crystallization process of the perovskite films with MPAT time from 5s to 35 s.

4. Conclusions

In summary, we have demonstrated a ambient processed hybrid treatment that combines advantages of microwave treatment followed by annealing (MPAT) to obtain reproducible, high quality $CH_3NH_3PbI_{3-x}Cl_x$ perovskite films in ambient environment without use of conventional antisolvent methods that requires mandatory and expensive glove-box processing. Improved quality of perovskite films after MPAT treatment is confirmed from the UV-Visible, X-ray diffraction studies and SEM images. The films prepared using MAPT treatment employed in inverted device architecture yield improved performance, reproducibility and less-hysteresis as compare to the films prepared without MPAT processing. The advantage and the mechanistic insights of MPAT on superior quality of perovskite films are beneficial for the use of the technique for large-scale fabrication of high-quality mixed halide films.

Conflicts of interest

There are no conflicts to declare.

Acknowledgements

The work was supported by the National Natural Science foundation of China (Nos. 61540016), the Natural Science foundation of Henan province (No.182300410241). S. M. J. acknowledge Marie Curie COFUND fellowship, Welsh Assembly Government funded Ser-Cymru Solar Project, European Union's Horizon 2020 research and innovation programme under the Marie Skłodowska-Curie grant agreement No 663830.

References

1. National Renewable Energy Labs (NREL) efficiency chart: http://www.nrel.gov/ncpv/images/efficiency-chart.jpg (accessed:January 2019)
2. A. Kojima, K. Teshima, Y. Shirai and T. Miyasaka, *Journal of the American Chemical Society*, 2009, **131**, 6050.
3. W. E. I. Sha, X. Ren, L. Chen and W. C. H. Choy, *Applied Physics Letters*, 2015, **106**, 506-514.
4. Q. Wang, C. C. Chuneh, M. Eslamian and A. K. Y.Jen, *Applied Materials Interfaces*, 2016, 8, 32068-32076.
5. G. E. Eperon, V. M. Burlakov, P. Docampo, A. Goriely and H. J. Snaith, *Advanced Functional Materials*, 2014, **24**, 151-157.
6. H.-B. Kim, H. Choi, J. Jeong, S. Kim, B. Walker, S. Song and J. Y. Kim, *Nanoscale*, 2014, **6**, 6679-6683.
7. J. H. Noh, S. H. Im, J. H. Heo, T. N. Mandal and S. I. Seok, *Nano Letters*, 2013, **13**, 1764-1769.
8. S. Ameen, M. A. Rub, S. A. Kosa, K. A. Alamry, M. S. Akhtar, H. S. Shin, H. K. Seo, A. M. Asiri and M. K. Nazeeruddin, *ChemSusChem*, 2016, **9**, 10-27.
9. H. D. Pham, Z. Wu, L. K. Ono, S. Manzhos, K. Feron, N. Motta, Y. Qi and P. Sonar, *Advanced Electronic Materials*, 2017, **3**, 1700139.
10. X. Zhao and M. Wang, *Materials today energy*, 2018, **7**, 208-220.
11. S. M. Jain, Z. Qiu, L. Häggman, M. Mirmohades, M. B. Johansson, T. Edvinsson and G. Boschloo, *Energy & Environmental Science*, 2016, **9**, 3770-3782.
12. S. M. Jain, B. Philippe, E. M. Johansson, B.-w. Park, H. Rensmo, T. Edvinsson and G. Boschloo, *Journal of Materials Chemistry A*, 2016, **4**, 2630-2642.
13. A. Dualeh, N. Tétreault, T. Moehl, P. Gao, M. K. Nazeeruddin and M. Grätzel, *Advanced Functional Materials*, 2014, **24**, 3250-3258.
14. J. Xiao, Y. Yang, X. Xu, J. Shi, L. Zhu, S. Lv, H. Wu, Y. Luo, D. Li and Q. Meng, *Journal of Materials Chemistry A*, 2015, **3**, 5289-5293.
15. J. Liu, C. Gao, X. He, Q. Ye, L. Ouyang, D. Zhuang, C. Liao, J. Mei and W. Lau, *Acs Applied Materials & Interfaces*, 2015, **7**, 24008-24015.
16. Z. Xiao, Q. Dong, C. Bi, Y. Shao, Y. Yuan and J. Huang, *Advanced Materials*, 2014, **26**, 6503-6509.
17. D. Gutiérrez-Tauste, I. Zumeta, E. Vigil, M. A. Hernández-Fenollosa, X. Domènech and J. A. Ayllón, *Journal of photochemistry and photobiology A: chemistry*, 2005, **175**, 165-171.
18. Ahmadian-Yazdi M R, Eslamian M. Materials Today Communications, 2018, 14: 151-159.
19. Xiong H, Zabihi F, Wang H, et al. Nanoscale, 2018, 10(18): 8526-8535.
20. Ahmadian-Yazdi M R, Habibi M, Eslamian M. Applied Sciences, 2018, 8(2): 308.
21. R. T. Hitchcock, Radio-frequency and microwave radiation, AIHA, 2004.

22. S. Kumar and S. Shukla, *Concepts and Applications of MICROWAVE ENGINEERING*, PHI Learning Pvt. Ltd., 2014.
23. G. A. Jones, D. H. Layer and T. G. Osenkowsky, *National Association of Broadcasters Engineering Handbook: NAB Engineering Handbook*, Taylor & Francis, 2013.
24. H. Ma, W.-W. Liu, X. Chen, Y.-J. Wu and Z.-L. Yu, *Bioresource Technology*, 2009, **100**, 1279-1284.
25. Z. Hu and Z. Wen, *Biochemical Engineering Journal*, 2008, **38**, 369-378.
26. D. Jackowiak, J. Frigon, T. Ribeiro, A. Pauss and S. Guiot, *Bioresource technology*, 2011, **102**, 3535-3540.
27. X. Lu, B. Xi, Y. Zhang and I. Angelidaki, *Bioresource technology*, 2011, **102**, 7937-7940.
28. X.-w. XU, F. YIN, R. XU, J.-c. LI, S.-q. LIU, Y.-b. CHEN and W.-d. ZHANG, *Liquor-Making Science & Technology*, 2009, **10**, 025.
29. Q. YE, Z. ZHI-Cheng and X.-w. GE, *Polymeric Materials Science & Engineering*, 2004, **3**, 003.
30. H. Jiangli, *Environmental Engineering*, 2002, **5**, 007.
31. Q. Hu, L. Zhao, J. Wu, K. Gao, D. Luo, Y. Jiang, Z. Zhang, C. Zhu, E. Schaible and A. Hexemer, *Nature communications*, 2017, **8**, 15688.
32. M.-F. Xu, H. Zhang, S. Zhang, H. L. Zhu, H.-M. Su, J. Liu, K. S. Wong, L.-S. Liao and W. C. Choy, *Journal of Materials Chemistry A*, 2015, **3**, 14424-14430.
33. H. Zhou, Q. Chen, G. Li, S. Luo, T.-b. Song, H.-S. Duan, Z. Hong, J. You, Y. Liu and Y. Yang, *Science*, 2014, **345**, 542-546.
34. M. Habibi, A. Rahimzadeh and M. Eslamian, *Eur Phys J E Soft Matter*, 2016, **39**, 30.
35. M. M. Maitani, D. Iso, J. Kim, S. Tsubaki and Y. Wada, *Electrochemistry*, 2017, **85**, 236-240.
36. D. Voiry, J. Yang, J. Kupferberg, R. Fullon, C. Lee, H. Y. Jeong, H. S. Shin and M. Chhowalla, *Science*, 2016, **353**, 1413-1416.
37. W. Zhu, C. Bao, Y. Wang, F. Li, X. Zhou, J. Yang, B. Lv, X. Wang, T. Yu and Z. Zou, *Dalton Transactions*, 2016, **45**, 7856-7865.
38. H. Hu, Z. Zhao, Q. Zhou, Y. Gogotsi and J. Qiu, *Carbon*, 2012, **50**, 3267-3273.
39. Q. Cao, S. Yang, Q. Gao, L. Lei, Y. Yu, J. Shao and Y. Liu, *ACS Appl Mater Interfaces*, 2016, **8**, 7854-7861.
40. M.-F. Xu, H. Zhang, S. Zhang, H. L. Zhu, H.-M. Su, J. Liu, K. S. Wong, L.-S. Liao and W. C. H. Choy, *Journal of Materials Chemistry A*, 2015, **3**, 14424-14430.
41. Xu M F, Zhang H, Zhang S, et al. Journal of Materials Chemistry A, 2015, 3(27): 14424-14430.
42. J. Hu, R. Gottesman, L. Gouda, A. Kama, M. Priel, S. Tirosh, J. Bisquert and A. Zaban, *ACS Energy Letters*, 2017, **2**, 950-956.
43. L. Bertoluzzi, R. S. Sanchez, L. Liu, J.-W. Lee, E. Mas-Marza, H. Han, N.-G. Park, I. Mora-Sero and J. Bisquert, *Energy & Environmental Science*, 2015, **8**, 910-915.
44. Q. Cao, S. Yang, Q. Gao, L. Lei, Y. Yu, J. Shao and Y. Liu, *ACS applied materials & interfaces*, 2016, **8**, 7854-7861.
45. R. Gottesman, P. Lopez-Varo, L. Gouda, J. A. Jimenez-Tejada, J. Hu, S. Tirosh, A. Zaban and J. Bisquert, *Chem*, 2016, **1**, 776-789.
46. W. Q. Wu, F. Huang, D. Chen, Y. B. Cheng and R. A. Caruso, *Advanced Functional Materials*, 2015, **25**, 3264-3272.
47. C. Li, Q. Guo, W. Qiao, Q. Chen, S. Ma, X. Pan, F. Wang, J. Yao, C. Zhang and M. Xiao, *Organic Electronics*, 2016, **33**, 194-200.
48. O. Vazquez-Mena, J. P. Bosco, O. Ergen, H. I. Rasool, A. Fathalizadeh, M. Tosun, M. Crommie, A. Javey, H. A. Atwater and A. Zettl, *Nano letters*, 2014, **14**, 4280-4285.
49. I. Hussain, M. Y. Soomro, N. Bano, O. Nur and M. Willander, *Journal of Applied Physics*, 2012, **112**, 064506.